

# Object-Centric Latent Action Learning

Albina Klepach<sup>\*,1</sup> Alexander Nikulin<sup>1,2</sup> Ilya Zisman<sup>1,3</sup> Denis Tarasov<sup>1,4</sup>  
Alexander Derevyagin<sup>1</sup> Andrei Polubarov<sup>1,3</sup> Nikita Lyubaykin<sup>1,5</sup> Vladislav Kurenkov<sup>1,5</sup>

<sup>1</sup>AIRI, <sup>2</sup>MIPT, <sup>3</sup>Skoltech, <sup>4</sup>ETH Zürich, <sup>5</sup>Innopolis University

## Abstract

Leveraging vast amounts of unlabeled internet video data for embodied AI is currently bottlenecked by the lack of action labels and the presence of action-correlated visual distractors. Although recent latent action policy optimization (LAPO) has shown promise in inferring proxy-action labels from visual observations, its performance degrades significantly when distractors are present. To address this limitation, we propose a novel object-centric latent action learning framework that centers on objects rather than pixels. We leverage self-supervised object-centric pretraining to disentangle action-related and distracting dynamics. This allows LAPO to focus on task-relevant interactions, resulting in more robust proxy-action labels, enabling better imitation learning and efficient adaptation of the agent with just a few action-labeled trajectories. We evaluated our method in eight visually complex tasks across the Distracting Control Suite (DCS) and Distracting MetaWorld (DMW). Our results show that object-centric pretraining mitigates the negative effects of distractors by **50%**, as measured by downstream task performance: average return (DCS) and success rate (DMW).

## 1 Introduction

In recent years, the scaling of model and data sizes has led to the creation of powerful and general foundation models (Bommasani et al., 2021) that have enabled many breakthroughs in understanding and generation of natural language (Achiam et al., 2023; Brown et al., 2020) and images (Dehghani et al., 2023; Radford et al., 2021). In contrast, the field of embodied AI has generally remained behind in terms of generalization and emergent abilities, being mostly limited by the lack of diverse high-quality data for pre-training (Guruprasad et al., 2024; Lin et al., 2024). The vast amount of video data on the Internet, covering a wide variety of human-related activities, can potentially fulfill the current data needs for training generalist agents (McCarthy et al., 2024). Unfortunately, such videos cannot be used directly due to lack of explicit action labels, which are essential for imitation learning and reinforcement learning algorithms.

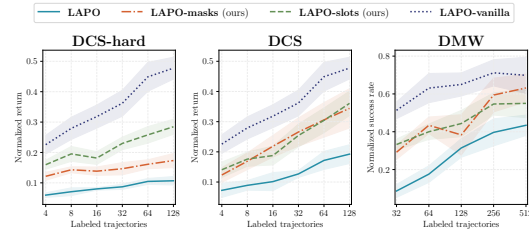


Figure 1: **Main Results.** We achieve significant downstream performance improvements across all environments and budgets of action-labeled trajectories considered. We normalize returns and success rates by the performance of the BC agent trained on the all ground-truth action labels. LAPO-vanilla uses data without distractors, representing the upper bound performance. Results averaged over three random seeds. See Section 4 for additional details.

\*Correspondence: klepach@airi.net. Work by dunnolab.ai.

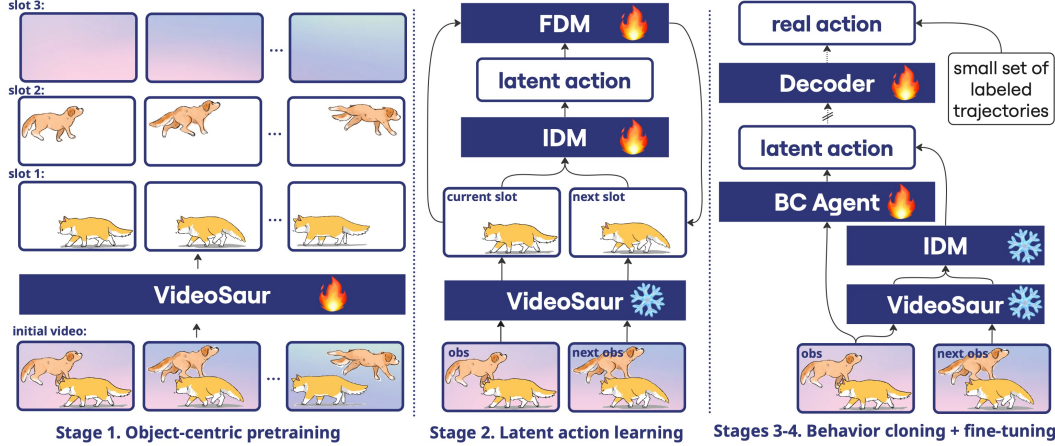


Figure 2: General overview of the our method pre-training pipeline. **Object-Centric Pretraining:** We decompose video sequences into interpretable object slots. A linear probe trained on slot representations automatically selects task-relevant slots by identifying those most predictive of actions. **Latent Action Learning:** We train a latent action model based on LAPO, learning inverse and forward dynamics in the slot space. **Behavior Cloning and Fine-tuning:** A behavior cloning agent is trained on the inferred latent actions. The resulting policy is then fine-tuned using a small number of trajectories with ground-truth actions ( $\leq 2.5\%$  of total data), enabling strong downstream performance with minimal supervision.

In order to compensate for the lack of action labels, approaches based on Latent Action Models (LAMs) (Schmidt & Jiang, 2024; Ye et al., 2024; Cui et al., 2024; Bruce et al., 2024), aim to infer latent actions from the sequence of visual observations. Such latent actions can later be used for behavioral cloning from large unlabeled datasets. However, a major limitation of current LAM approaches, is their susceptibility to action-correlated distractors, such as dynamic backgrounds, that falsely correlate with agent actions, and may lead models to overfit to non-causal patterns (Wang et al., 2024; Misra et al., 2024b; McCarthy et al., 2024; Nikulin et al., 2025). Existing methods, such as Latent Action Pretraining (LAPA) (Ye et al., 2024; Chen et al., 2024), often assume curated, distractor-free datasets or rely on costly annotations, severely limiting their scalability and applicability in realistic settings.

To address this bottleneck, we propose object-centric latent action learning, a framework that leverages object-centric representations to isolate task-relevant entities from distracting visual noise. Object-centric models decompose scenes into discrete, interpretable object slots (Locatello et al., 2020; Dittadi et al., 2022) using self-supervised mechanisms that group pixels into coherent entities based on feature similarity. These slots encode spatio-temporal properties (Zadaianchuk et al., 2023) effectively disentangling complex visual inputs into semantically meaningful units.

Our core hypothesis is that **object-centric representations provide the necessary structural priors to separate causal agent-object interactions from non-causal visual correlations**. By operating on slot-based object features rather than raw pixels, our method enables LAMs to focus on the dynamics of relevant objects while filtering out distractions such as background motion.

We evaluated our approach in continuous control environments with dynamic distractors, such as Distracting Control Suite (DCS) (Stone et al., 2021) and previously unexplored Distracting Metaworld (DMW) (Yu et al., 2019), showing that self-supervised object-centric pretraining, built on VideoSAUR (Zadaianchuk et al., 2023), significantly improves robustness compared to standard LAM baselines. Our results suggest that object decomposition serves as an effective inductive bias for latent action learning, especially under realistic, noisy conditions. In addition, we propose a simple way to automatically choose slots relevant to control and analyze its effectiveness. We summarize our main results on Figure 1.

## 2 Preliminaries

In our experiments, we use environments with partial observability (POMDP) (Åström, 1965; Kaelbling et al., 1998). A POMDP is defined by the tuple  $(\mathcal{S}, \mathcal{A}, T, R, \Omega, \gamma)$ , where:  $\mathcal{S}$  is the state

space,  $\mathcal{A}$  is the action space,  $T(s_{t+1} | s_t, a_t)$  defines the transition dynamics,  $R(s_t, a_t, s_{t+1})$  is the reward function,  $\Omega(o_t | s_t)$  is the observation model,  $\gamma \in [0, 1]$  is the discount factor. At each time step  $t$ , the agent receives an observation,  $o_t \sim \Omega(\cdot | s_t)$ , and selects an action  $a_t \sim \pi(\cdot | o_t)$  to maximize its expected discounted return:  $\mathbb{E} [\sum_{k=t}^{\infty} \gamma^{k-t} r_k]$ . The agent transitions to the next state  $s_{t+1} \sim T(\cdot | s_t, a_t)$  and receives a reward  $r_t = R(s_t, a_t, s_{t+1})$ .

We consider the setting in which we first learn a policy  $\pi$  from offline demonstration data, then fine-tune it through online interaction introduced by Schmidt & Jiang (2024). Suppose we are given a dataset  $\mathcal{D}$  of expert trajectories in the form of sequences of observations and actions:

$$\tau_{oa} = \{(o_0, a_0, o_1), \dots, (o_{|\tau|-1}, a_{|\tau|-1}, o_{|\tau|})\}$$

When such labeled data is available, Behavior Cloning (BC) (Pomerleau, 1988) can be used to train a policy  $\pi_{BC}(a_t | o_t)$  through supervised learning. However, when using real-world video data the action labels are missing, and we only observe sequences of the form:

$$\tau_o = \{o_0, o_1, \dots, o_{|\tau|}\}$$

**Latent Action Modeling.** Edwards et al. (2019); Schmidt & Jiang (2024) proposed to convert classic BC into a pseudo-BC task by inferring latent actions  $z_t$  that explain each observed transition  $(o_t, o_{t+1})$ . These inferred actions are then used to train a latent action policy  $\tilde{\pi}(z_t | o_t)$ , bypassing the need for ground-truth action labels. To obtain latent actions, LAM trains an inverse-dynamics model (IDM)  $f_{IDM}(z_t | o_t, o_{t+1})$ , which infers latent actions from state transitions. To ensure that the IDM learns meaningful representations, it is trained jointly with a forward-dynamics model (FDM):  $f_{FDM}(o_{t+1} | o_t, z_t)$ , which predicts the next observation from the current observation and the inferred action. The models are optimized to perform next observation prediction:

$$\mathcal{L}_{MSE} = \mathbb{E}_t [\|f_{FDM}(f_{IDM}(o_t, o_{t+1}), o_t) - o_{t+1}\|^2]$$

Without distractors LAM is able to recover ground-truth actions (Schmidt & Jiang, 2024; Bruce et al., 2024), however, with distractions it does not work (Nikulin et al., 2025).

**Challenge of distractors.** Real-world videos inherently contain action-correlated distractors: environmental dynamics (e.g. moving backgrounds, camera jitter) that spuriously correlate with agent actions. However, existing learning from observation (LfO) methods lack mechanisms to disentangle distractors (Efroni et al., 2022; Misra et al., 2024a), leading to overfitting in noisy settings. Recently, Nikulin et al. (2025) empirically demonstrated that LAPO-based methods suffer significant performance degradation when trained on data that contain distractors and suggested reusing available action labels to provide supervision during LAM pre-training. However, it is not always possible to provide such supervision, since action labels do not exist in principle in some domains (e.g. YouTube videos). On the other hand, object-centric decomposition can be applied in a meaningful way to any real-world video data, greatly expanding the applicability of latent action learning.

**Object-Centric Decomposition.** Object-centric learning (OCL) aims to decompose complex visual scenes into structured, interpretable representations by isolating individual entities over time. These entities are typically encoded as a set of  $K$  slot vectors  $\mathcal{S}_t = \{s_t^{(1)}, s_t^{(2)}, \dots, s_t^{(K)}\}$ , representing a distinct entity or region within the scene and capture object-specific properties such as position, shape, color, and motion. A key strength of OCL models lies in their ability to encode the causal structure of the environment. By isolating coherent, temporally consistent entities, they provide a natural defense against distractors in real-world video data. For example, VideoSAUR (Zadaianchuk et al., 2023), a self-supervised video decomposition model, has been shown to effectively ignore spurious correlations introduced by moving backgrounds or viewpoint changes, focusing instead on task-relevant objects.

Although object slots provide disentangled and semantically meaningful representations, identifying which slots correspond to task-relevant entities remains challenging and necessitates additional mechanisms to identify and track relevant entities without manual supervision. Also, most OCL frameworks, including VideoSAUR, require the number of slots  $K$  to be specified a priori, which limits flexibility in modeling scenes with varying numbers of objects and can lead to either under-representation or fragmentation when  $K$  is mismatched with scene complexity.

### 3 Method

**Object-Centric Representation Learning.** We employ the VideoSAUR model (Zadaianchuk et al., 2023) to decompose input video frames into spatio-temporal object slots. We initially experimented with the STEVE model (Singh et al., 2022), a widely used and promising approach, but found that it failed to consistently isolate entities such as the hopper in our tasks (illustrated compared to VideoSAUR in Figure 25).

VideoSaur’s self-supervised architecture isolates individual entities within a scene, providing structured representations that are less susceptible to background noise and incidental motion. At the end of this step, we obtain an encoder, that directly maps a trajectory of observations  $\tau_o = (o_1, \dots, o_T)$  to a corresponding trajectory of slots  $\tau_s = (s_1, \dots, s_T)$ . VideoSAUR encodes each observation  $o_t$  in a fixed number  $K$  of slot vectors  $s_t^{(k)} \in \mathbb{R}^d$ , where the parameter  $K$  is set prior to training.

Due to its transformer-based decoder, VideoSAUR allows each slot  $s_t^{(k)}$  to be projected back into the original observation space using attention maps as alpha masks. This enables us to visualize and interpret the spatial support of each slot in the image. We denote these by  $m_t^{(k)}$  and refer to them as object masks throughout the paper (see Figures 3, 25 and 26 for visualizations).

To improve consistency between training runs and reduce slot permutation issues, we employ fixed initialization of slots (see details in Appendix C), which ensures that the same slot index corresponds to a similar semantic object across different episodes.

**Slot Selection.** In our setting, control-relevant objects typically include the main agent (e.g. cheetah in "cheetah-run" from DCS, robotic arm and gripper from DWM) and some objects (hammer, cubes, etc. in DMW), depending on the environment and the number of slots  $K$ , these entities can occupy one or more slots. To identify which slots correspond to the agent’s interactions, we propose an automated method to select relevant slots based on their relationship to inferred actions, inspired by Alain & Bengio (2016). A linear regressor is trained to predict ground-truth actions from fixed slot encodings on a small number of labeled trajectories. We apply Principal Component Analysis (PCA) to slot encodings beforehand to reduce dimensionality and noise.

To ensure robustness and reduce variance in performance estimates, we use 5-fold cross-validation and report the average mean squared error (MSE) on the test data, as the final evaluation metric. Slots with lower MSE are considered to be more predictive of the true action and thus more likely to represent control-relevant entities. We select a subset of top- $N$  slots with the lowest prediction error as our final set of relevant slots  $\mathcal{S}_t^* = \{s_t^{(k)} \mid k \in \mathcal{K}^*\}$ , where  $\mathcal{K}^*$  denotes the indices of selected slots. This selection process is performed once per dataset due to the fixed initialization of slots, ensuring consistent interpretation across episodes.



Figure 3: Visuals from Distraction Control Suite. From top to bottom: cheetah-run, walker-run, hopper-hop, humanoid-walk. From left to right: the distracted observation (background video, color, and camera position variations), the non-distracted observation, the mixture of slot decoder masks obtained after object-centric pretraining, and the main object slot decoder mask selected after object-centric pretraining.

**Latent Action Modeling.** Utilizing the selected object-centric representations, we train a latent action model inspired by LAPO (Schmidt & Jiang, 2024) under the space of object-centric representations. The inverse-dynamics model  $z_t \sim f_{\text{IDM}}^s(\cdot | s_t, a_{t+1})$  and the forward-dynamics model  $\hat{s}_{t+q} \sim f_{\text{FDM}}^s(\cdot | s_t, z_t)$  are trained to reconstruct the trajectory of slots  $\|\hat{s}_{t+1} - s_{t+1}\|^2$  (or masks). We denote this as **LAPO-slots** and, accordingly, **LAPO-masks** for masks representations. Thus, LAPO-slots reconstruct next observations in latent space, while LAPO-masks reconstruct images, which were filtered based on selected slots (see Figures 3 and 26).

Table 1: Normalized evaluation returns (DCS) and normalized success rates (DMW) of the BC agent trained on latent actions for different tasks. TL;DR: LAPO’s performance drops in the presence of distractors. Object-centric learning, using slots and masks, reduces this gap. Each value represents the average score across different amounts of fine-tuning labeled trajectories and three random seeds. The BC agent trained with access to the full dataset of ground-truth actions would achieve a score of 1 for each task. The relative performance gain is given as  $\frac{\text{LAPO} - \text{LAPO-slots/masks}}{\text{LAPO} - \text{LAPO-vanilla}}$ .

Task	LAPO baseline	LAPO-vanilla upper-bound	LAPO-masks ours		LAPO-slots ours	
cheetah-run	0.24 ± 0.02	0.76 ± 0.04	0.41 ± 0.03	+32%	0.55 ± 0.04	+58%
hopper-hop	0.03 ± 0.01	0.27 ± 0.03	0.08 ± 0.01	+20%	0.15 ± 0.02	+50%
walker-run	0.04 ± 0.01	0.32 ± 0.07	0.06 ± 0.01	+6%	0.12 ± 0.01	+27%
humanoid-walk	0.02 ± 0.01	0.06 ± 0.01	0.04 ± 0.02	+47%	0.06 ± 0.01	+105%
<b>Mean DCS-hard</b>	0.08 ± 0.01	0.35 ± 0.04	0.15 ± 0.02	<b>+26%</b>	0.22 ± 0.02	<b>+52%</b>
cheetah-run	0.34 ± 0.06	0.76 ± 0.04	0.54 ± 0.09	+48%	0.50 ± 0.07	+38%
hopper-hop	0.05 ± 0.01	0.27 ± 0.03	0.15 ± 0.01	+46%	0.19 ± 0.02	+64%
walker-run	0.10 ± 0.01	0.32 ± 0.07	0.21 ± 0.05	+52%	0.18 ± 0.03	+36%
humanoid-walk	0.02 ± 0.01	0.06 ± 0.01	0.05 ± 0.02	+67%	0.09 ± 0.02	+174%
<b>Mean DCS</b>	0.13 ± 0.02	0.35 ± 0.04	0.24 ± 0.04	<b>+50%</b>	0.24 ± 0.03	<b>+50%</b>
hammer	0.75 ± 0.07	0.98 ± 0.01	0.96 ± 0.01	+91%	0.99 ± 0.02	+102%
bin-picking	0.18 ± 0.08	0.74 ± 0.10	0.49 ± 0.10	+56%	0.33 ± 0.08	+27%
basketball	0.17 ± 0.03	0.51 ± 0.07	0.34 ± 0.09	+50%	0.37 ± 0.09	+58%
soccer	0.14 ± 0.06	0.36 ± 0.08	0.21 ± 0.08	+34%	0.23 ± 0.06	+41%
<b>Mean DMW</b>	0.31 ± 0.06	0.65 ± 0.06	0.50 ± 0.07	<b>+55%</b>	0.48 ± 0.06	<b>+50%</b>

**Behavior Cloning and Finetuning.** The inferred latent actions serve as proxies for actual action labels. We train a behavior cloning (BC) agent to predict these latent actions, using the same dataset as for latent action learning. To evaluate the pre-training effectiveness, as a final stage, we fine-tune the resulting agent on a limited set of trajectories with ground-truth action labels (no more than 2.5% of total data), in line with (Schmidt & Jiang, 2024; Ye et al., 2024; Nikulin et al., 2025). The BC agent scores for different numbers of labeled trajectories are presented on Figure 4.

## 4 Experiments

Our experiments are designed to address the following core questions: **(1) Can object-centric representations disentangle task-relevant motion from distracting visual elements?** **(2) How much supervision is needed to train effective latent action models under high visual distraction?** **(3) Can we automate slot selection to reduce the dependency on domain expertise or manual annotation?**

### 4.1 Datasets

We evaluate our approach using two benchmark environments: one focused on control tasks under distractions (DCS) and another involving multi-object manipulation (DMW). More details on dataset collection can be found in Appendix A.

**Distracting Control Suite (DCS).** The DCS environment (Stone et al., 2021) extends DeepMind Control with three types of real-world visual noise: (1) dynamic backgrounds: 60 diverse videos from DAVIS 2017 (Pont-Tuset et al., 2018), simulating realistic environmental clutter; (2) color variations: hue/saturation shifts that preserve object semantics but degrade low-level features; (3) camera perturbations: randomized pose adjustments mimicking handheld camera noise. We mainly focused on dynamic backgrounds (marked as **DCS**), but also showed the results on all 3 types of distraction (marked as **DCS-hard**) in Figures 1 and 7 and Table 1. We study four locomotion tasks ordered by complexity: cheetah-run, walker-run, hopper-hop, and humanoid-walk. We trained experts



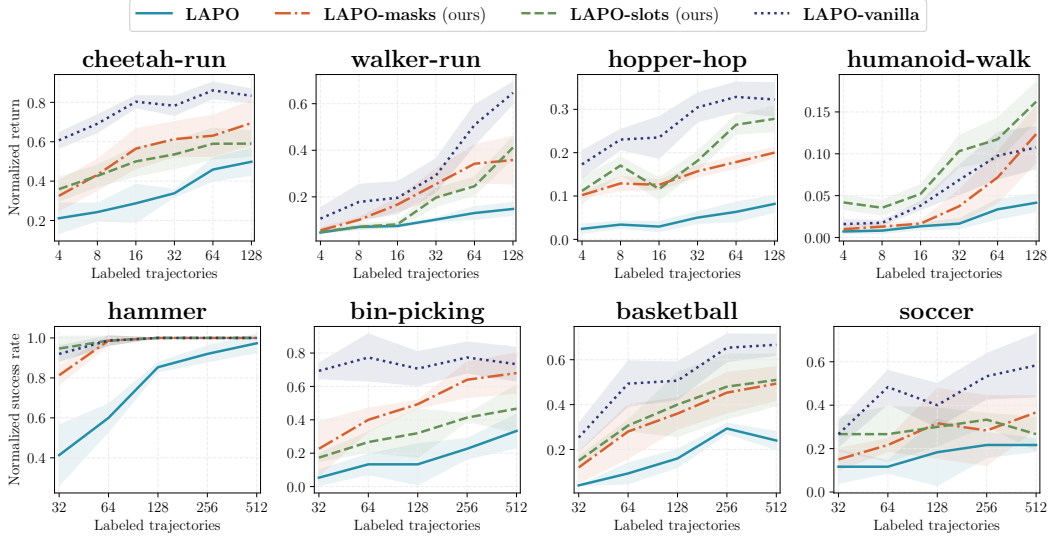


Figure 4: Normalized evaluation returns and success rates of the BC agent trained on latent actions for varying numbers of fine-tuning labeled trajectories. TL;DR: Object-centric learning improves evaluation returns in DCS tasks and success rate in goal-based DMW task for all tasks. The plots are arranged from left to right in order of increasing task complexity. The values are averaged across three random seeds. The BC agent trained with access to the full dataset of ground-truth actions would return a score of 1 for each task.

on privileged state information and collected the dataset with observation-action tuples. Importantly, the behavior cloning agent, trained on privileged true actions, is able to achieve expert score (Table 2).

**Distracting MetaWorld (DMW).** The DMW environment extends MetaWorld with dynamic backgrounds, replicating the DCS setting. MetaWorld is a goal-based robotic multi-object benchmark featuring complex interactions between multiple objects. To our knowledge, MetaWorld with background distractions has not been previously explored. Tasks include hammer, bin-picking, basketball, and soccer. These tasks emphasize compositional reasoning and object interaction, allowing us to assess multi-object scenarios. The experts were taken from MetaWorlds’s oracle policies.

## 4.2 Setup

To conduct the experiments, 4 models were trained: **LAPO**, **LAPO-vanilla**, **LAPO-slots** and **LAPO-masks**. All models were trained on the same datasets. More details on training can be found in Appendix B.

**Baseline.** The baseline model is LAPO, which is trained on observations with distractors, following the Schmidt & Jiang (2024) procedure (**LAPO** in the figures). We use it as a baseline to demonstrate the currently existing limitations of latent action pretraining.

**Upper bound.** We also trained LAPO on clean data without distractors as our second baseline to illustrate the performance gap caused by distractors (**LAPO-vanilla** in the figures).

**Our approaches.** LAPO-slots and LAPO-masks are the models that follow the object-centric latent action pre-training training pipeline described in Section 3 (respectively, **LAPO-slots** and **LAPO-masks** in the figures). LAPO-slots uses slot embeddings extracted from VideoSAUR as input to the latent action model, LAPO-masks uses slot masks, treating each mask as an attention map applied to the original frame.

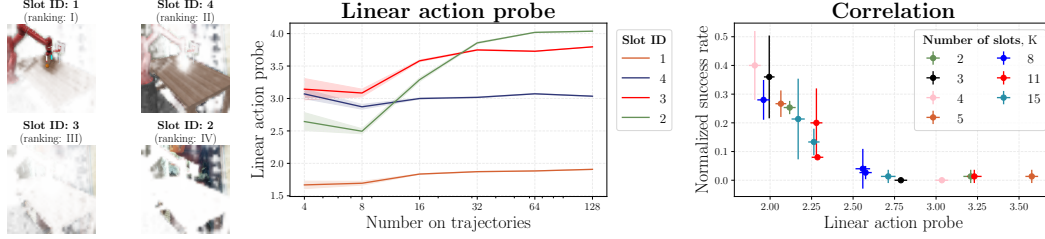


Figure 5: Slot selection investigation. From left to right: (1) Corresponding slot masks for basketball task after VideoSaur pretraining for number of slots  $K = 4$ . (2) Linear action probes for VideoSaur slots pretrained basketball task for varying budget of trajectories. (3) Linear action probes and corresponding resulting normalized success rates of BC agents on 128 labeled trajectories for different number of slots (top-2 slots for  $K \leq 5$ , top-3 slots for  $K \geq 8$ ).

### 4.3 Evaluation performance

To assess the quality of learned latent actions, we train a BC agent  $\pi_{BC}(a_t | z_t)$  on the inferred latent actions  $z_t$ , then fine-tune it on a small number of trajectories (0.1% – 2.5% from the entire dataset) with true action labels. The small size of the action-labeled sample mirrors real-world deployment, where labeling is expensive. The final performance is measured as **normalized episodic return** for DCS and **normalized success rate** for DMW, where a score of 1 corresponds to an oracle BC policy (see Table 2) trained on the entire dataset with ground-truth actions.

**Quantitative Results.** As shown in Table 1, both LAPO-slots and LAPO-masks strongly outperform the standard LAPO baseline for both the DCS and DMW domains. Notably: In DCS, LAPO-slots improves the gap between LAPO performance with and without distractors by 50% on average, with even greater gains in complex tasks like ‘humanoid-walk’ (+174%). In DMW, the improvements are consistent, with LAPO-slots achieving a +50% improvement on average over the baseline. These results support our hypothesis: object-centric representations help filter out distractors and retain actionable information. Figure 4 shows evaluation returns across increasing numbers of fine-tuning trajectories. Both slot-based methods show better generalization from fewer labeled examples.

### 4.4 Slot selection investigation

A major benefit of object-centric modeling lies in its ability to attribute dynamics to specific entities. However, identifying which slots correspond to control-relevant entities remains a challenge. We explore whether linear probes trained to predict ground-truth actions from slot representations can identify relevant slots automatically. The detailed explanation of the technique is given in Section 3. This method shows strong agreement with manual selection and correlates well with downstream performance (see Figure 5 and Appendices E to H), suggesting that slot probing can serve as a reliable proxy for slot relevance.

Interestingly, we observe that meaningful task-related information tends to concentrate among the top-1 or top-2 slots (Figure 6). Specifically: for  $K \leq 8$ , only the top-1 slot contributes non-zero evaluation scores. For larger  $K$  values ( $K = 11$  and  $K = 15$ ), the top-2 slots capture most of the useful signal. Aggregating the two most relevant slots through concatenation leads to improved performance (??), compared to using each slot individually. This suggests that meaningful information is distributed across these two slots.

### 4.5 Varying number of slots

The number of slots  $K$  is a critical hyperparameter in object-centric models like VideoSAUR (Zadachuk et al., 2023), directly influencing both representation quality and downstream performance. Although prior work has explored adaptive slot allocation strategies (Fan et al., 2024), most object-centric approaches still rely on a fixed  $K$ , typically selected based on the expected complexity of the scene.

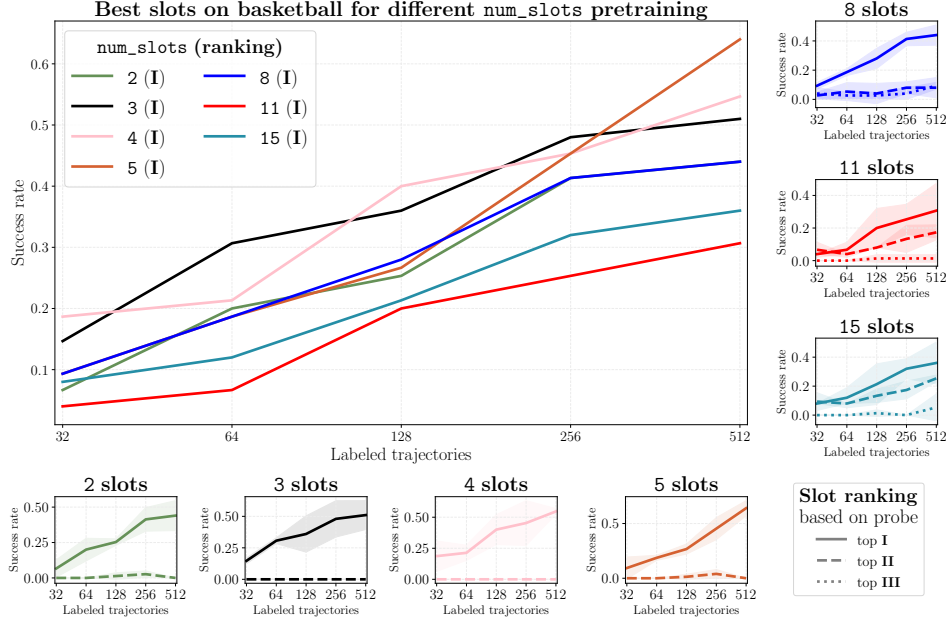


Figure 6: Normalized success rates of the BC agent trained on latent actions for varying numbers of fine-tuning labeled trajectories across a range of slot counts from  $K = 2$  to  $K = 15$  on DMW tasks. Slots are ranked based on linear probe scores. TL;DR: Automatic probe selection correlates well with downstream performance. The values are averaged across three random seeds. The BC agent trained with access to the full dataset of ground-truth actions would return a score of 1 for each task.

We evaluated LAPO-slots across a range of slot counts from  $K = 2$  to  $K = 15$  on DMW tasks. As shown in Figure 6, performance generally improves as  $K$  increases, reaching its peak at 3–5 slots, after which it declines. Too few slots lead to collapsed representations in which multiple entities are merged into one, while too many introduce noise, redundancy, and instability (see Appendix H for visualizations). For instance, we observe "duplicating" slots (nearly identical representations) for  $K \geq 5$ , e.g., for  $K = 5$ , only two unique slots emerge (for  $K = 8$  four distinct slots, for  $K = 11$  or  $K = 15$  only seven).

Interestingly, when applied to DMW, we expected a clear separation of distinct objects such as the robotic arm, hammer, ball, etc. Instead, VideoSAUR grouped these task-relevant entities into a single slot even when the number of slots  $K$  was greater than the amount of objects. We attribute this behavior to limited diversity in expert trajectories: within each task, variation arises primarily from changes in the initial position of the manipulated object (e.g., hammer or ball), with no variation in the initial position of the arm or target object. This lack of data diversity likely limits the incentive for fine-grained decomposition and highlights a key limitation of current object-centric models: they struggle to disentangle objects meaningfully when the underlying data lack sufficient variability in object interactions or spatial configurations. It also shows that the setting of our study reflects real-world conditions, where data is rarely perfectly diverse or balanced.

#### 4.6 Increasing distractions difficulty

To better understand how different types of visual distractions impact latent action learning, we evaluate our methods under increasingly challenging conditions in the Distracting Control Suite (DCS) (Stone et al., 2021) environment. In this work, we primarily focus on dynamic backgrounds as the core challenge, but we also test combinations of all three distractor types (backgrounds, camera position, and color variations) on DCS (marked DCS-hard on Figure 1 and Table 1) to assess robustness.



As shown in Figure 1, all methods suffer performance degradation under additional distractors, for example, LAPO performance drops by  $\times 2.7$  under background distractions and by  $\times 4.4$  under additional distractors, compared to the performance without distractors. However, LAPO-slots maintains a consistent relative improvement over baseline (50% on DCS  $\rightarrow$  52% on DCS-hard), while LAPO-masks degrades (50% on DCS  $\rightarrow$  26% on DCS-hard).

This difference probably stems from VideoSAUR’s use of the DINOv2 encoder Oquab et al. (2023), which captures high-level semantic features and is more robust to appearance changes than the CNN-based encoder in LAPO and LAPO-masks. These findings suggest that slot-based representations not only isolate task-relevant entities but also encode objects using features that generalize better under real-world visual perturbations.

## 5 Related work

Vision-Language-Action (VLA) models have emerged as a powerful paradigm for embodied AI, with recent advances focusing on latent action representations to enhance their capabilities. Ye et al. (2024) uses latent actions by pretraining VLM to predict latent actions from text prompt, enabling unsupervised pretraining of VLA models for robotic manipulation. Genie (Bruce et al., 2024) is a foundational world model, trained from unlabeled videos, which can generate interactive environments from images. Recently, Bu et al. (2025) trained cross-embodiment VLA policies for manipulation and navigation. They use LAM to derive task-centric action representations from videos.

Villar-Corrales & Behnke (2025) explores the application of object-centric representations for latent action learning and video prediction, showing positive results in robotic tabletop simulations. In contrast to our work, Villar-Corrales & Behnke (2025) does not explore the limitations of such an approach to latent action learning in the presence of distractors, similar to existing research. Moreover, instead of VideoSAUR (Zadachuk et al., 2023) employed in our work, their method uses SAVi (Kipf et al., 2021) for object-centric learning, which, as we show (see Appendix J) does not work well in more complex environments with real-world distractors.

Nikulin et al. (2025) focuses on latent action learning under distractors, closely aligned with ours. Even though the topic is the same, the method, presented by the authors is orthogonal. It presents a latent action framework without reconstruction which shows improvement with distractors, however, utilizes supervision (small dataset of labeled trajectories) during pre-training.

Together, these works highlight the growing interest in robust latent action learning under visual distractions. Our contribution uniquely bridges object-centric perception and latent action modeling, emphasizing slot stability, interpretability, and reduced supervision requirements.

## 6 Conclusion & Limitations

Our results demonstrate that object-centric representations significantly mitigate the impact of distractors in learning latent actions from videos. By disentangling scene elements into meaningful, interpretable slots, latent actions focus on causal dynamics rather than spurious correlations. This could provide a strong inductive bias for more effective Latent Action Models in noisy environments. However, several limitations remain that constrain the applicability and scalability of current object-centric frameworks.

Despite being unsupervised, object-centric models like VideoSAUR do not offer direct control over what is learned. Although we successfully automate slot selection using linear probing, this process still requires access to a small set of labeled trajectories to train the probe itself. Similarly, while latent action learning benefits from large-scale unlabeled video data, fine-tuning on expert-labeled trajectories remains essential for achieving strong downstream performance. Future work may explore other directions for incorporating weak supervision.

A key limitation we observe is the sensitivity of object-centric models to dataset composition. In robotic manipulation tasks, such as DMW, the limited diversity in expert trajectories leads to collapsed object representations. A promising direction towards mitigating data diversity issue is the use of generative approaches (Luo et al., 2025; Sikchi et al., 2024) to augment the dataset, enabling models to learn more robust and generalizable object decompositions through knowledge transfer.

A major limitation of current slot-based video models like VideoSAUR is the lack of memory mechanisms, which restricts modeling dynamic scenes where objects may enter or leave the scene over time. This issue becomes especially important in long-horizon sequences involving occlusions, multi-object interactions, or complex environments. Recent attempts to address this include dictionary-based slot architectures and hierarchical slot structures (Đukić et al.), but these remain early-stage and mostly limited to image-level processing rather than full video understanding. Furthermore, most OCL methods operate under the assumption of a known and fixed number of objects  $K$ , limiting their ability to model hierarchical structures or scenes with varying numbers of objects.

## References

- Josh Achiam, Steven Adler, Sandhini Agarwal, Lama Ahmad, Ilge Akkaya, Florencia Leoni Aleman, Diogo Almeida, Janko Altenschmidt, Sam Altman, Shyamal Anadkat, et al. Gpt-4 technical report. *arXiv preprint arXiv:2303.08774*, 2023. 1
- Guillaume Alain and Yoshua Bengio. Understanding intermediate layers using linear classifier probes. *arXiv preprint arXiv:1610.01644*, 2016. 4
- Karl Johan Åström. Optimal control of markov processes with incomplete state information i. *Journal of mathematical analysis and applications*, 10:174–205, 1965. 2
- Rishi Bommasani, Drew A Hudson, Ehsan Adeli, Russ Altman, Simran Arora, Sydney von Arx, Michael S Bernstein, Jeannette Bohg, Antoine Bosselut, Emma Brunskill, et al. On the opportunities and risks of foundation models. *arXiv preprint arXiv:2108.07258*, 2021. 1
- Tom Brown, Benjamin Mann, Nick Ryder, Melanie Subbiah, Jared D Kaplan, Prafulla Dhariwal, Arvind Neelakantan, Pranav Shyam, Girish Sastry, Amanda Askell, et al. Language models are few-shot learners. *Advances in neural information processing systems*, 33:1877–1901, 2020. 1
- Jake Bruce, Michael D Dennis, Ashley Edwards, Jack Parker-Holder, Yuge Shi, Edward Hughes, Matthew Lai, Aditi Mavalankar, Richie Steigerwald, Chris Apps, et al. Genie: Generative interactive environments. In *Forty-first International Conference on Machine Learning*, 2024. 2, 3, 9
- Qingwen Bu, Yanting Yang, Jisong Cai, Shenyuan Gao, Guanghui Ren, Maoqing Yao, Ping Luo, and Hongyang Li. Univla: Learning to act anywhere with task-centric latent actions. *arXiv preprint arXiv:2505.06111*, 2025. 9
- Xiaoyu Chen, Junliang Guo, Tianyu He, Chuheng Zhang, Pushi Zhang, Derek Cathera Yang, Li Zhao, and Jiang Bian. Igor: Image-goal representations are the atomic control units for foundation models in embodied ai. *arXiv preprint arXiv:2411.00785*, 2024. 2
- Zichen Jeff Cui, Hengkai Pan, Aadithya Iyer, Siddhant Haldar, and Lerrel Pinto. Dynamo: In-domain dynamics pretraining for visuo-motor control. *arXiv preprint arXiv:2409.12192*, 2024. 2
- Mostafa Dehghani, Josip Djolonga, Basil Mustafa, Piotr Padlewski, Jonathan Heek, Justin Gilmer, Andreas Peter Steiner, Mathilde Caron, Robert Geirhos, Ibrahim Alabdulmohsin, et al. Scaling vision transformers to 22 billion parameters. In *International Conference on Machine Learning*, pp. 7480–7512. PMLR, 2023. 1
- Andrea Dittadi, Samuele Papa, Michele De Vita, Bernhard Schölkopf, Ole Winther, and Francesco Locatello. Generalization and robustness implications in object-centric learning. In *International Conference on Machine Learning*, 2022. 2
- Ashley Edwards, Himanshu Sahni, Yannick Schroecker, and Charles Isbell. Imitating latent policies from observation. In *International conference on machine learning*, pp. 1755–1763. PMLR, 2019. 3
- Yonathan Efroni, Dipendra Misra, Akshay Krishnamurthy, Alekh Agarwal, and John Langford. Provable rl with exogenous distractors via multistep inverse dynamics, 2022. URL <https://arxiv.org/abs/2110.08847>. 3
- Ke Fan, Zechen Bai, Tianjun Xiao, Tong He, Max Horn, Yanwei Fu, Francesco Locatello, and Zheng Zhang. Adaptive slot attention: Object discovery with dynamic slot number. In *Proceedings of the IEEE/CVF Conference on Computer Vision and Pattern Recognition*, pp. 23062–23071, 2024. 7
- Pranav Guruprasad, Harshvardhan Sikka, Jaewoo Song, Yangyue Wang, and Paul Pu Liang. Benchmarking vision, language, & action models on robotic learning tasks. *arXiv preprint arXiv:2411.05821*, 2024. 1

- Leslie Pack Kaelbling, Michael L Littman, and Anthony R Cassandra. Planning and acting in partially observable stochastic domains. *Artificial intelligence*, 101(1-2):99–134, 1998. 2
- Thomas Kipf, Gamaleldin F Elsayed, Aravindh Mahendran, Austin Stone, Sara Sabour, Georg Heigold, Rico Jonschkowski, Alexey Dosovitskiy, and Klaus Greff. Conditional object-centric learning from video. *arXiv preprint arXiv:2111.12594*, 2021. 9
- Thomas Kipf, Gamaleldin F. Elsayed, Aravindh Mahendran, Austin Stone, Sara Sabour, Georg Heigold, Rico Jonschkowski, Alexey Dosovitskiy, and Klaus Greff. Conditional object-centric learning from video, 2022. URL <https://arxiv.org/abs/2111.12594>. 20
- Fanqi Lin, Yingdong Hu, Pingyue Sheng, Chuan Wen, Jiacheng You, and Yang Gao. Data scaling laws in imitation learning for robotic manipulation. *arXiv preprint arXiv:2410.18647*, 2024. 1
- Francesco Locatello, Dirk Weissenborn, Thomas Unterthiner, Aravindh Mahendran, Georg Heigold, Jakob Uszkoreit, Alexey Dosovitskiy, and Thomas Kipf. Object-centric learning with slot attention. *Advances in neural information processing systems*, 33:11525–11538, 2020. 2
- Calvin Luo, Zilai Zeng, Yilun Du, and Chen Sun. Solving new tasks by adapting internet video knowledge. *arXiv preprint arXiv:2504.15369*, 2025. 9
- Robert McCarthy, Daniel CH Tan, Dominik Schmidt, Fernando Acero, Nathan Herr, Yilun Du, Thomas G Thuruthel, and Zhibin Li. Towards generalist robot learning from internet video: A survey. *arXiv preprint arXiv:2404.19664*, 2024. 1, 2
- Dipendra Misra, Akanksha Saran, Tengyang Xie, Alex Lamb, and John Langford. Towards principled representation learning from videos for reinforcement learning, 2024a. URL <https://arxiv.org/abs/2403.13765>. 3
- Dipendra Misra, Akanksha Saran, Tengyang Xie, Alex Lamb, and John Langford. Towards principled representation learning from videos for reinforcement learning. *arXiv preprint arXiv:2403.13765*, 2024b. 2
- Alexander Nikulin, Ilya Zisman, Denis Tarasov, Nikita Lyubaykin, Andrei Polubarov, Igor Kiselev, and Vladislav Kurenkov. Latent action learning requires supervision in the presence of distractors. *arXiv preprint arXiv:2502.00379*, 2025. 2, 3, 5, 9
- Maxime Oquab, Timothée Darcet, Theo Moutakanni, Huy V. Vo, Marc Szafraniec, Vasil Khalidov, Pierre Fernandez, Daniel Haziza, Francisco Massa, Alaaeldin El-Nouby, Russell Howes, Po-Yao Huang, Hu Xu, Vasu Sharma, Shang-Wen Li, Wojciech Galuba, Mike Rabbat, Mido Assran, Nicolas Ballas, Gabriel Synnaeve, Ishan Misra, Herve Jegou, Julien Mairal, Patrick Labatut, Armand Joulin, and Piotr Bojanowski. Dinov2: Learning robust visual features without supervision, 2023. 9, 13
- Dean A Pomerleau. Alvin: An autonomous land vehicle in a neural network. *Advances in neural information processing systems*, 1, 1988. 3
- Jordi Pont-Tuset, Federico Perazzi, Sergi Caelles, Pablo Arbeláez, Alex Sorkine-Hornung, and Luc Van Gool. The 2017 davis challenge on video object segmentation, 2018. URL <https://arxiv.org/abs/1704.00675>. 5
- Alec Radford, Jong Wook Kim, Chris Hallacy, Aditya Ramesh, Gabriel Goh, Sandhini Agarwal, Girish Sastry, Amanda Askell, Pamela Mishkin, Jack Clark, et al. Learning transferable visual models from natural language supervision. In *International conference on machine learning*, pp. 8748–8763. PMLR, 2021. 1
- Dominik Schmidt and Minqi Jiang. Learning to act without actions. In *The Twelfth International Conference on Learning Representations*, 2024. URL <https://arxiv.org/abs/2312.10812>. 2, 3, 4, 5, 6
- Harshit Sikchi, Siddhant Agarwal, Pranaya Jajoo, Samyak Parajuli, Caleb Chuck, Max Rudolph, Peter Stone, Amy Zhang, and Scott Niekum. RL zero: Zero-shot language to behaviors without any supervision. *arXiv preprint arXiv:2412.05718*, 2024. 9
- Gautam Singh, Yi-Fu Wu, and Sungjin Ahn. Simple unsupervised object-centric learning for complex and naturalistic videos. *Advances in Neural Information Processing Systems*, 35:18181–18196, 2022. URL <https://arxiv.org/abs/2205.14065>. 4, 20
- Austin Stone, Oscar Ramirez, Kurt Konolige, and Rico Jonschkowski. The distracting control suite – a challenging benchmark for reinforcement learning from pixels, 2021. URL <https://arxiv.org/abs/2101.02722>. 2, 5, 8

- Nikola Đukić, Tim LeBailly, and Tinne Tuytelaars. Ocebo: Object-centric pretraining by target encoder bootstrapping. In *The Thirteenth International Conference on Learning Representations*. 10
- Angel Villar-Corrales and Sven Behnke. Playslot: Learning inverse latent dynamics for controllable object-centric video prediction and planning, 2025. URL <https://arxiv.org/abs/2502.07600>. 9
- Yucen Wang, Shenghua Wan, Le Gan, Shuai Feng, and De-Chuan Zhan. Ad3: Implicit action is the key for world models to distinguish the diverse visual distractors. *arXiv preprint arXiv:2403.09976*, 2024. 2
- Ross Wightman. Pytorch image models. <https://github.com/rwightman/pytorch-image-models>, 2019. 13
- Seonghyeon Ye, Joel Jang, Byeongguk Jeon, Sejune Joo, Jianwei Yang, Baolin Peng, Ajay Mandlekar, Reuben Tan, Yu-Wei Chao, Bill Yuchen Lin, Lars Liden, Kimin Lee, Jianfeng Gao, Luke Zettlemoyer, Dieter Fox, and Minjoon Seo. Latent action pretraining from videos, 2024. URL <https://arxiv.org/abs/2410.11758>. 2, 5, 9
- Tianhe Yu, Deirdre Quillen, Zhanpeng He, Ryan Julian, Karol Hausman, Chelsea Finn, and Sergey Levine. Meta-world: A benchmark and evaluation for multi-task and meta reinforcement learning. In *Conference on Robot Learning (CoRL)*, 2019. URL <https://arxiv.org/abs/1910.10897>. 2
- Andrii Zadaianchuk, Maximilian Seitzer, and Georg Martius. Object-centric learning for real-world videos by predicting temporal feature similarities. In *Thirty-seventh Conference on Neural Information Processing Systems*, 2023. URL <https://openreview.net/forum?id=t1jLRFvBqm>. 2, 3, 4, 7, 9, 13

## A Dataset collection

**Distracting Control Suite (DCS):** The datasets were collected via experts policies trained on DCS via PPO (for cheetah-run, walker-run and hopper-hop) and SAC (for humanoid-walk). The scores of the experts are presented on the Table 2. The final dataset of transitions for each tasks consists of 5k trajectories (1k transitions each). The observations in the dataset have height and width 64px.

**Distracting MetaWorld (DMW):** The datasets were collected via experts policies from MetaWorld. The scores of the experts are presented on the Table 2. The final dataset of transitions for each tasks consists of 20k successfull trajectories (we filtered out non-successfull trajectories during dataset collection). The observations in the dataset have height and width 128px.

Table 2: Comparison of the Performance of Algorithms. **Expert** denotes the policy used to collect the dataset trained on privileged information about minimal state of the observation (DCS) and expert policy from (DMW). **BC-vanilla** denotes the scores of behavior cloning agents (BC) trained on full expert dataset to imitate expert policy on the privileged for our method true action labels and non-distracted observations. **BC** denotes the scores of BC agents trained on full expert dataset to imitate expert policy on the distracted observations and privileged for our method true action labels.

Task	Expert policy	Expert dataset	BC-vanilla	BC	Size, GB
cheetah-run	838	838	840	823	58
walker-run	740	740	735	749	58
hopper-hop	307	307	300	253	58
humanoid-walk	617	617	601	428	59
hammer	1.0	1.0	1.0	1.0	61
bin-picking	1.0	1.0	1.0	1.0	114
basketball	0.96	1.0	1.0	1.0	87
soccer	0.88	1.0	1.0	0.8	67

## B Training details

All experiments were run in H100 GPU 80GB. The models are trained in bfloat16 precision. Training duration is shown in Table 4. We perform hyperparameter optimization for each model. The 3 best sets of parameters were evaluated and the best mean score across 3 seeds is reported in Figure 4.

Object-centric learning pretraining codebase was adopted from Videosaur Zadaianchuk et al. (2023). It utilizes DINOv2 (Oquab et al., 2023) pretrained encoder vit-base-patch14-dinov2.lvd142m from Timm (Wightman, 2019) models hub. The images in the dataset are upscaled for dino encoder up to 518px. The hyperparameters for object-centric pretraining can be found in Table 5

Latent action learning model for images and object-centric masks is formed from IDM and FDM models based on a ResNet-like CNN encoder and decoder. The hyperparameter optimization setups for latent action learning from images (used for lapo, lapo-masks) can be found in Table 7.

Latent action learning model for object-centric slots is formed from IDM and FDM based on 3-layer MLP blocks with residual connections and GeLU activations to effectively process vector representations. The hyperparameter optimizations setups for latent action learning from representations (used for lapo-slots) can be found in Table 7.

## C Fixed Initialization for Slot Stability

To mitigate slot permutation variance across predictions, we introduce a fixed slot initialization scheme that learns deterministic initial slot vectors while preserving robustness. Unlike standard Gaussian initialization, which samples slots stochastically at each step, our approach learns per-slot parameters (mean  $\mu_k \in \mathbb{R}^d$  and variance  $\sigma_k \in \mathbb{R}^d$ ) during training. During training, we inject controlled noise scaled by the learned variance into the slot initializations, acting as a regularizer

to encourage robust feature disentanglement. At inference, slots are initialized deterministically using the learned means, ensuring consistent slot-object assignments. This hybrid strategy bridges the gap between training stability and inference consistency: the noise-augmented training phase prevents overfitting to fixed initializations, while the deterministic inference phase enables efficient object-wise slot selection via decoder masks as visual priors.

$$\text{Train: } \mathbf{s}_k^{(\text{init})} = \boldsymbol{\mu}_k + \boldsymbol{\sigma}_k \odot \boldsymbol{\epsilon}, \quad \boldsymbol{\epsilon} \sim \mathcal{N}(\mathbf{0}, \mathbf{I}), \quad \text{Inference: } \mathbf{s}_k^{(\text{inference})} = \boldsymbol{\mu}_k.$$

Table 3: Amount of parameters for different models. The rows represent the following approaches: **ocp**: denotes the number of parameters of the object-centric model; **lapo-slots**: denotes the number of parameters for latent action learning from vector representations; utilizing object-centric representations from a precollected dataset; **lapo**: denotes the number of parameters for latent action learning from images; **lapo-masks**: denotes the number of parameters for latent action learning from images, utilizing object-centric masks from a precollected dataset (using the same model as **lapo**); **bc**: Denotes the number of parameters of the behavior cloning agent trained on latent actions.

Method	DCS	DMW
ocp (total)	92,149,776	92,149,776
ocp (trainable)	6,343,440	6,343,440
lapo-slots	89,186,432	15,491,776
lapo-masks	211,847,849	36,269,129
lapo	211,847,849	36,269,129
bc	107,541,504	126,703,872

Table 4: Average training duration of the methods. The row represent the following approaches: **ocp** denotes the time spent on object-centric pretraining stage which is common for both slots and masks; **lapo-masks** and **lapo-slots** denote the time spent on training latent action model, reading object-centric representations from a precollected dataset; **lapo** denote the time spent on training latent action model, **ocp + lapo-masks** and **ocp + lapo-slots** denote the time for full pipeline of object-centric latent action learning

Method	Training Duration DCS	Training Duration DMW
ocp	~ 6 h 30 m	~ 8 h 30 m
lapo-slots	~ 2 h 30 m	~ 1 h 30 m
lapo-masks	~ 7 h 30 m	~ 2 h 30 m
lapo	~ 7 h 30 m	~ 2 h 30 m
ocp + lapo-slots	~ 9 h 0 m	~ 10 h 0 m
ocp + lapo-masks	~ 14 h 0 m	~ 11 h 00 m
bc + finetuning	~ 3 h 2 m	~ 1 h 30 m



## D Evaluation scores on DCS-hard

We mark as **DCS-hard**, the experiments on Distracting Control Suite with 3 types of distractions: dynamic backgrounds, color and camera position perturbations. The scale of color and camera variations is 0.1. The aggregated mean scores for DCS-hard are present on Figure 1 and Table 1.

The corresponding results on **DCS** (only dynamic backgrounds) are presented on Figures 1 and 4 and Table 1.

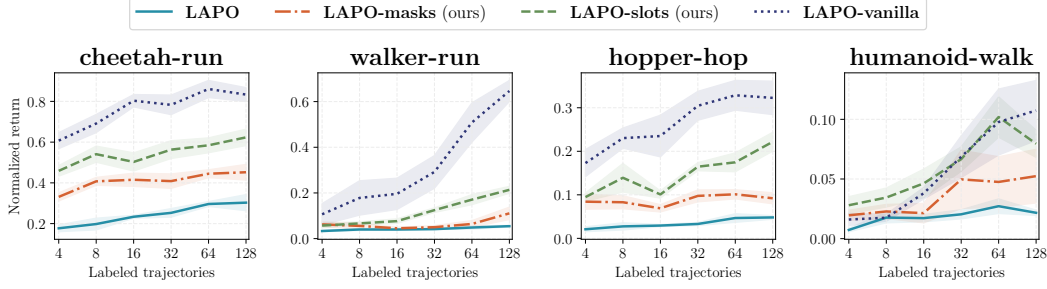


Figure 7: Normalized evaluation returns of the BC agent trained on latent actions for varying numbers of fine-tuning labeled trajectories. TL;DR: Object-centric learning improves evaluation returns in DCS tasks with all 3 types of distractions. The plots are arranged from left to right in order of increasing task complexity. The values are averaged across three random seeds. The BC agent trained with access to the full dataset of ground-truth actions would return a score of 1 for each task.

## E Correlation between probe and normalized success rates

We examine the correlation between the linear action probe (described in Section 3) and the evaluation performance, using the same budget of labeled trajectories for both probe training and supervised fine-tuning of object-centric latent action learning (LAPO-slots), on the basketball task from DMW.

As shown in Figure 8, there is a strong correlation between the probe performance and the resulting success rate, suggesting that the probe can serve as a reliable method for slot selection.

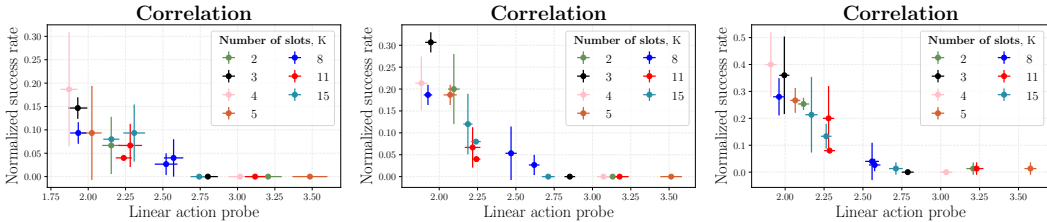


Figure 8: Linear action probes and corresponding resulting normalized success rates of BC agents on same amounts of labeled trajectories for different number of slots (top-2 slots for  $K \leq 5$ , top-3 slots for  $K \geq 8$ ). From left to right: (1) 32 labeled trajectories, (2) 64 labeled trajectories, (3) 128 labeled trajectories

## F Probe slots selection for DCS

Slot selection for tasks from Distracting Control Suite. The selected slots were used to obtain results for Figure 4 and Table 1.



Figure 9: Slot selection for **cheetah-run**. From left to right: (1) Linear action probes for VideoSaur slots pretrained cheetah-run task for varying budget of trajectories. (2) Corresponding slot masks for cheetah-run task after VideoSaur pretraining for number of slots  $K = 4$ .

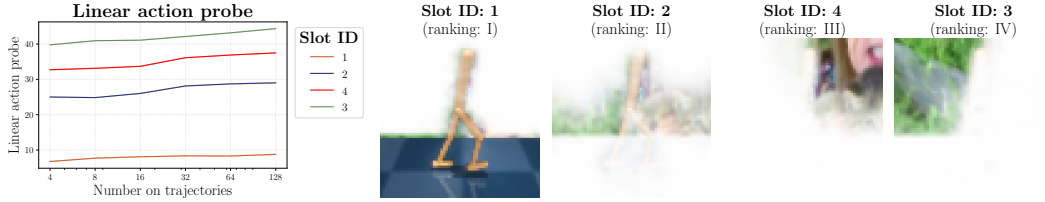


Figure 10: Slot selection for **walker-run**. From left to right: (1) Linear action probes for VideoSaur slots pretrained walker-run task for varying budget of trajectories. (2) Corresponding slot masks for walker-run task after VideoSaur pretraining for number of slots  $K = 4$ .

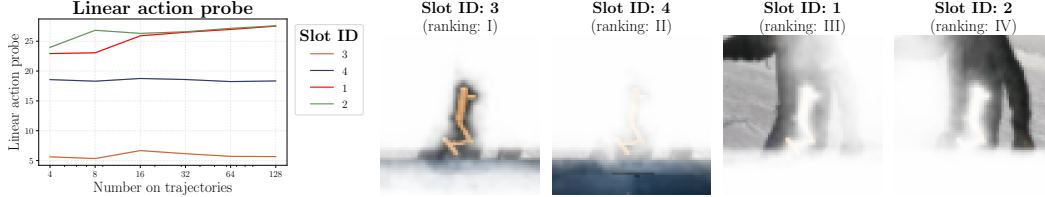


Figure 11: Slot selection for **hopper-hop**. From left to right: (1) Linear action probes for VideoSaur slots pretrained hopper-hop task for varying budget of trajectories. (2) Corresponding slot masks for hopper-hop task after VideoSaur pretraining for number of slots  $K = 4$ .

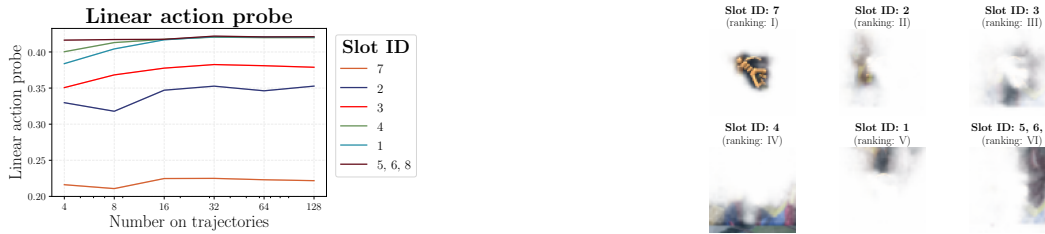


Figure 12: Slot selection for **humanoid-walk**. From left to right: (1) Linear action probes for VideoSaur slots pretrained humanoid-walk task for varying budget of trajectories. (2) Corresponding slot masks for humanoid-walk task after VideoSaur pretraining for number of slots  $K = 8$ .

## G Probe slots selection for DMW

Slot selection for tasks from Distracted MetaWord. The selected slots (ranking  $I$ ) were used to obtain results for Figure 4 and Table 1.

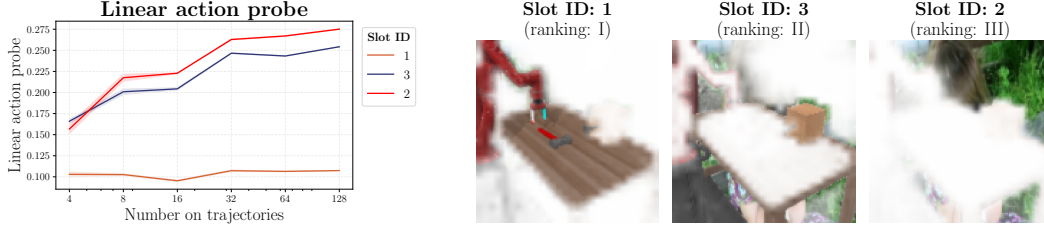


Figure 13: Slot selection for **hammer**. From left to right: (1) Linear action probes for VideoSaur slots pretrained hammer task for varying budget of trajectories. (2) Corresponding slot masks for hammer task after VideoSaur pretraining for number of slots  $K = 3$ .

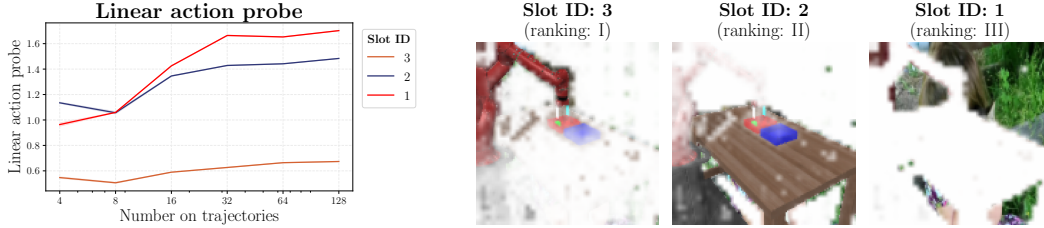


Figure 14: Slot selection for **bin-picking**. From left to right: (1) Linear action probes for VideoSaur slots pretrained bin-picking task for varying budget of trajectories. (2) Corresponding slot masks for bin-picking task after VideoSaur pretraining for number of slots  $K = 3$ .

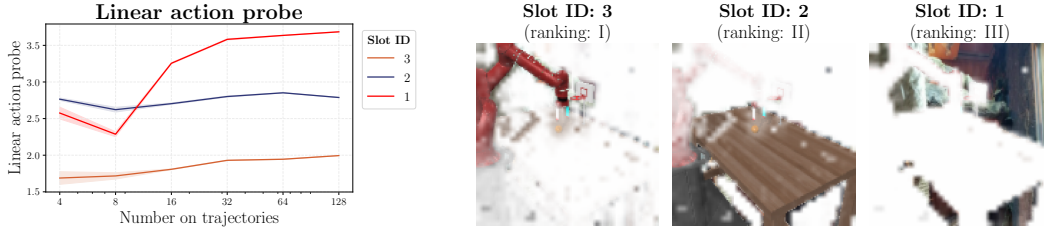


Figure 15: Slot selection for **basketball**. From left to right: (1) Linear action probes for VideoSaur slots pretrained basketball task for varying budget of trajectories. (2) Corresponding slot masks for basketball task after VideoSaur pretraining for number of slots  $K = 3$ .

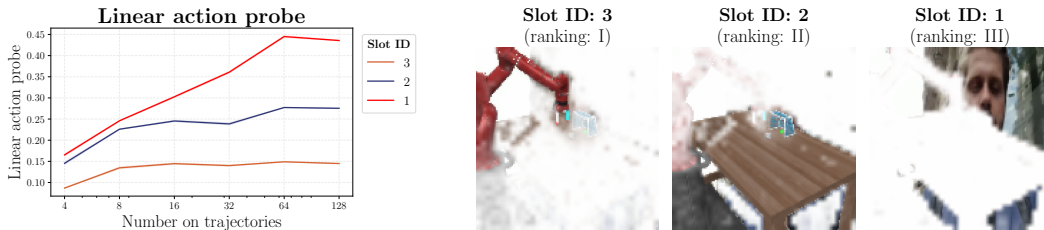


Figure 16: Slot selection for **soccer**. From left to right: (1) Linear action probes for VideoSaur slots pretrained soccer task for varying budget of trajectories. (2) Corresponding slot masks for soccer task after VideoSaur pretraining for number of slots  $K = 3$ .

## H Probe slots selection for different number of slots

Slot selection for varying number of slots for basketball task from Distracted MetaWord. The selected slots (ranking I) from Figures 15 and 18 to 22 were used to obtain the results for Figure 6.

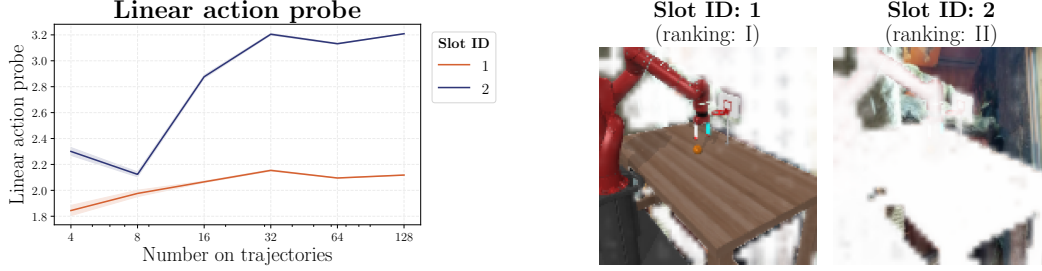


Figure 17: Slot selection for **2** slots. From left to right: (1) Linear action probes for VideoSaur slots pretrained basketball task for varying budget of trajectories. (2) Corresponding slot masks for basketball task after VideoSaur pretraining for number of slots  $K = 2$ .

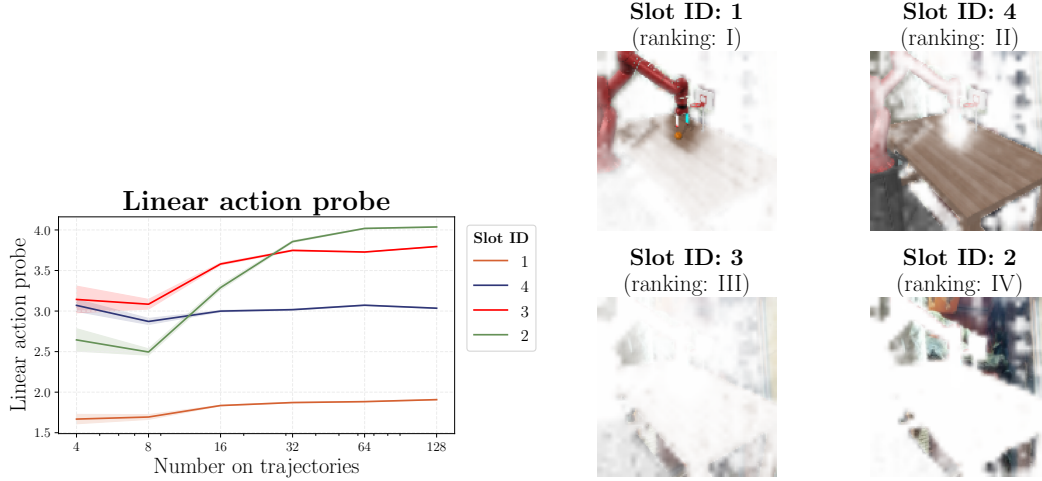


Figure 18: Slot selection for **4** slots. From left to right: (1) Linear action probes for VideoSaur slots pretrained basketball task for varying budget of trajectories. (2) Corresponding slot masks for basketball task after VideoSaur pretraining for number of slots  $K = 4$ .

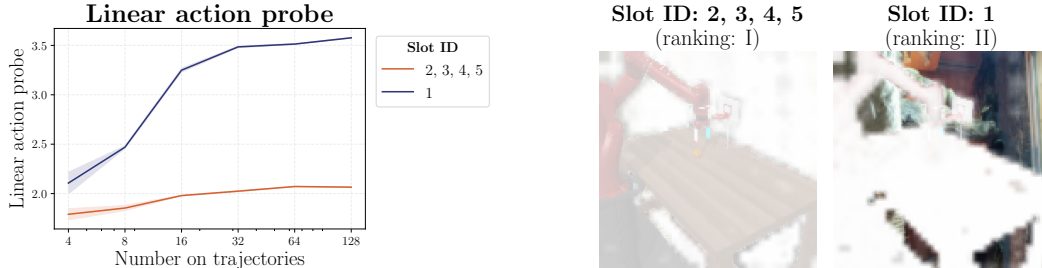


Figure 19: Slot selection for **5** slots. From left to right: (1) Linear action probes for VideoSaur slots pretrained basketball task for varying budget of trajectories. (2) Corresponding slot masks for basketball task after VideoSaur pretraining for number of slots  $K = 5$ .

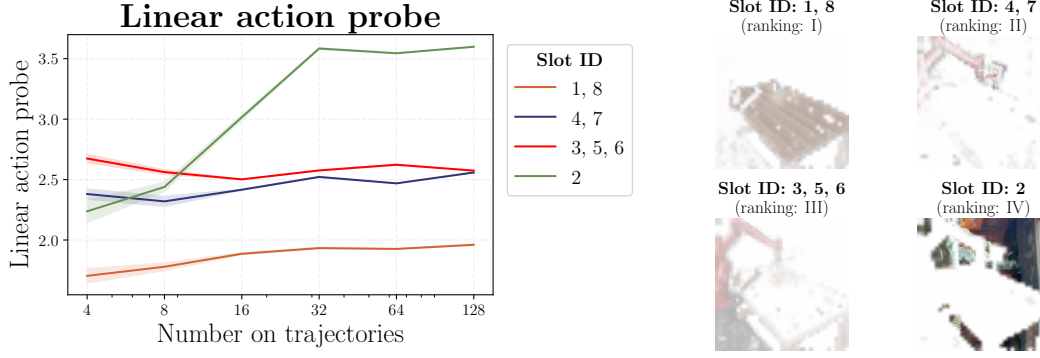


Figure 20: Slot selection for **8** slots. From left to right: (1) Linear action probes for VideoSaur slots pretrained basketball task for varying budget of trajectories. (2) Corresponding slot masks for basketball task after VideoSaur pretraining for number of slots  $K = 8$ .

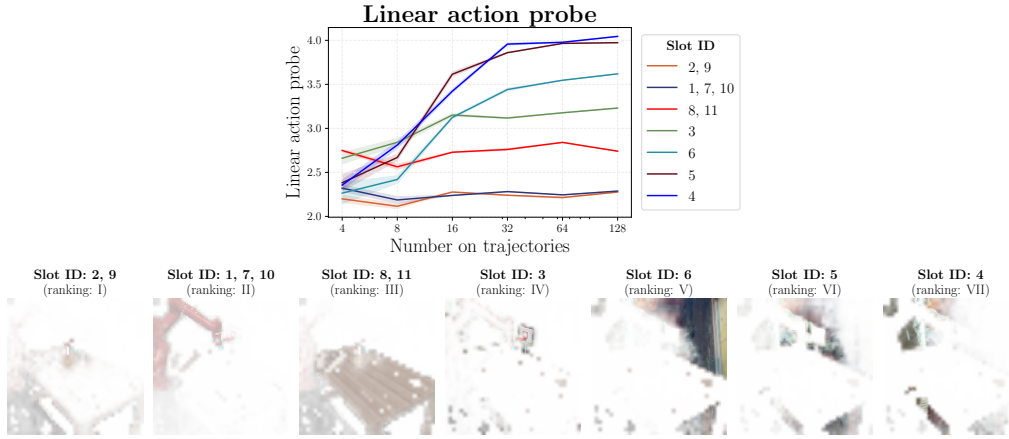


Figure 21: Slot selection for **11** slots. From top to bottom: (1) Linear action probes for VideoSaur slots pretrained basketball task for varying budget of trajectories. (2) Corresponding slot masks for basketball task after VideoSaur pretraining for number of slots  $K = 11$ .

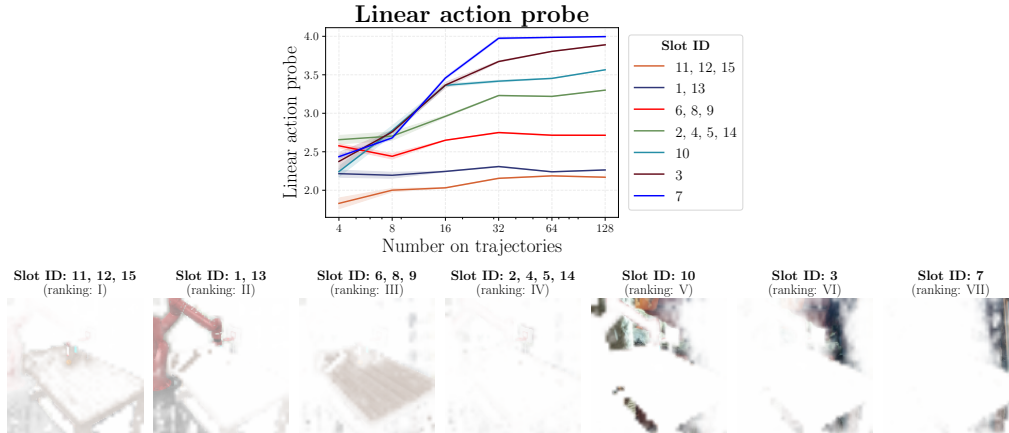


Figure 22: Slot selection for **15** slots. From top to bottom: (1) Linear action probes for VideoSaur slots pretrained basketball task for varying budget of trajectories. (2) Corresponding slot masks for basketball task after VideoSaur pretraining for number of slots  $K = 15$ .

## I Performance on aggregated slots

As shown in Figure 6, there is a noticeable drop in performance for  $K = 11$  and  $K = 15$  slots when selecting only the top-1 slot. Moreover, only the 11 slots and 15 slots configurations show non-zero performance on the top-2 slot. This suggests that meaningful information may be distributed across multiple slots rather than being concentrated in a single one. To investigate this further, we aggregated the two most relevant slots (the top-1 and top-2 slots) for both  $K = 11$  and  $K = 15$ . The results of this aggregation experiment are presented in Figure 23. These results indicate that aggregating the top two slots indeed leads to better performance, compared to using them individually, supporting the hypothesis that useful information is spread across multiple slots.

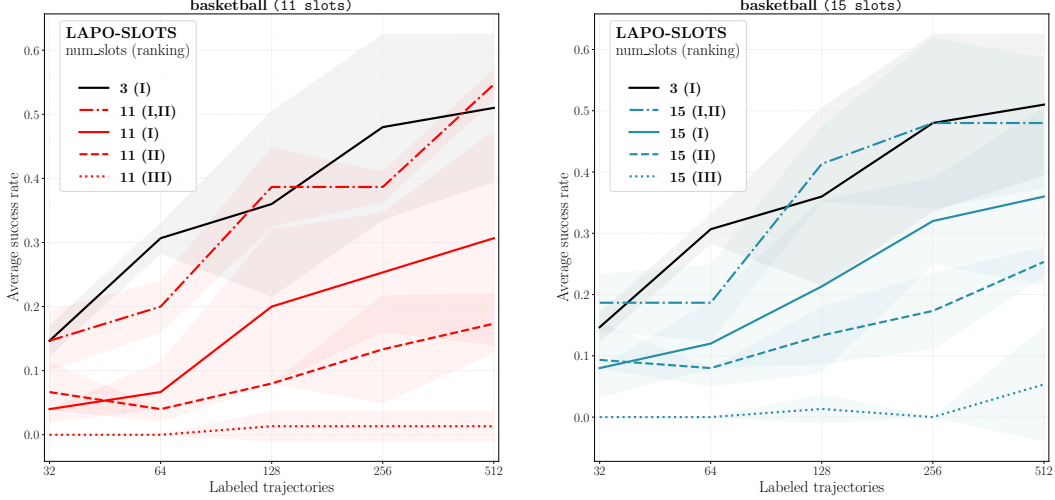


Figure 23: Normalized success rates of the BC agent trained on latent actions for varying numbers of fine-tuning labeled trajectories. From left to right: performance with number of slots  $K = 11$ ; performance with number of slots  $K = 15$ . **TL;DR**: Aggregation of top-2 slots for 11 and 15 slots, marked **11(I, II)** and, accordingly, **15(I, II)**, gives higher performance compared to performance on individual slots, marked **11(I)**, **11(II)**, **11(III)** and **15(I)**, **15(II)**, **15(III)**. Also we add a line **3(I)**, which denotes the performance on the selected slot on 3 slots (same as in Figure 4), to both plots for reference.

## J Comparing STEVE and VideoSAUR slot projections

We begin with the STEVE model (Singh et al., 2022), a widely adopted and promising approach for object-centric learning. However, we found that STEVE struggled to accurately identify the main object in visual inputs. In Figure 25, we compare the slot projections of STEVE and VideoSAUR, highlighting key differences in their representations. We also note that STEVE is largely similar to SAVi (Kipf et al., 2022), differing primarily in its use of a transformer-based decoder instead of a pixel-mixture decoder.

In terms of performance, we evaluate the STEVE-based object-centric model on the hopper-hop task from DCS (Figure 24), which underscores the importance of a strong object-centric representation for achieving good final performance.

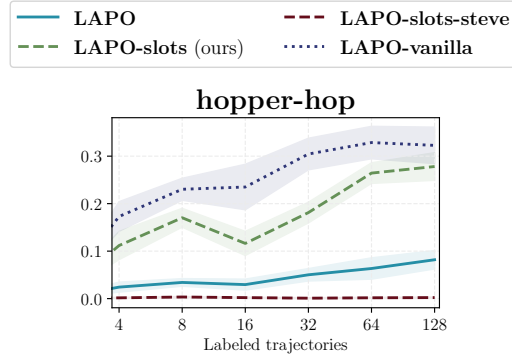


Figure 24: Normalized evaluation returns the BC agent trained on latent actions for varying numbers of fine-tuning labeled trajectories. **TL;DR**: Object-centric pretraining based on STEVE doesn't work.



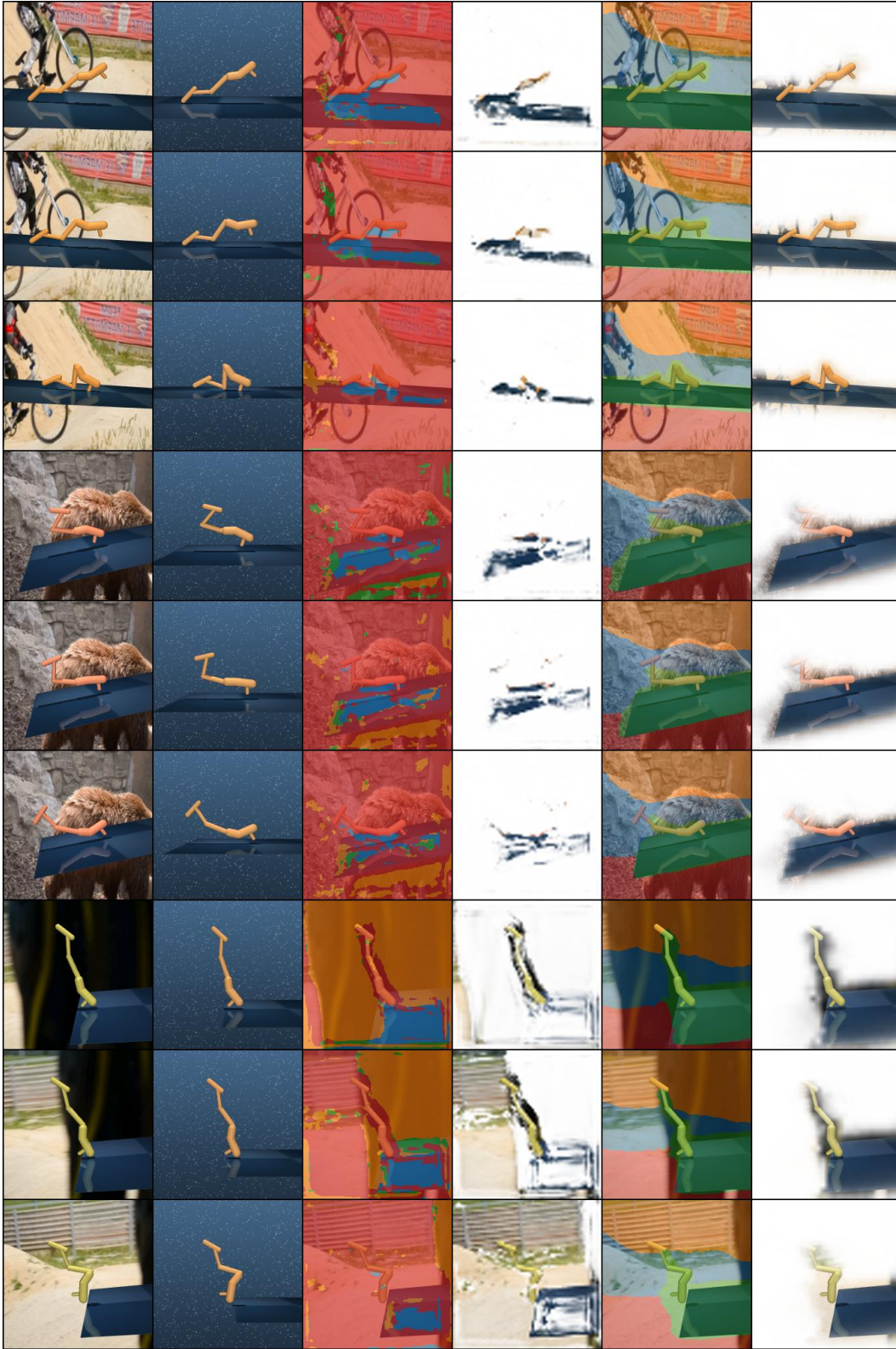


Figure 25: Examples of slot projections on DCS hopper-hop. From left to right: clean image without distractors, image with distractors, STEVE's slots projections, the main object's slot projection by STEVE, VideoSAUR's slot projections, the main object's slot by VideoSAUR

## K Examples of VideoSAUR slot projections on DCS-hard



Figure 26: Examples of VideoSAUR slot projections on DCS-hard for 4 tasks: (from upper to lower) cheetah-run, hopper-hop, walker-run, humanoid-walk. From left to right: distracted observation, clean observation, observation with segments of slot projections, slot projection (we call it "mask") of the main object

Table 5: Object-centric pretraining hyperparams. As for the number of slots: all DCS tasks were trained with 4 slots, except humanoid trained with 8 slots, all DMW tasks were trained with 3 slots for main tables.

Hyperparameter	Value
Episode Length	3
Image Size Dataset	64
Image Size Resize	224
Max Steps	100000
Batch Size	256
Warmup Steps	2500
Weight Decay	0
Max Video Length	1000
Gradient Clip Value	0.05
Slot Dimension	128
Vision Transformer Model	vit_base_patch8_224_dino
Feature Dimension	768
Number of Patches	784
Batch Size per GPU	128
Total Batch Size	128
Similarity Temperature	0.075
Similarity Weight	0.1
Base Learning Rate	0.0001
Learning Rate	0.0003
Learning Rate Scheduler	exp_decay_with_warmup
Warmup Steps	2500
Decay Steps	100000

Table 6: Hyperparameter optimization setups for latent action learning from vector representations (used for **lapo-slots**).

Hyperparameter	DCS	DMW
<b>Latent Action Learning</b>		
Batch Size	8192	64
Hidden Dimension	1024	1024
Num Blocks	3	[3, 5, 8]
Number of Epochs	30	30
Frame Stack	[1, 3]	[1, 3]
Weight Decay	0	0
Learning Rate	$\log(1e-3, 1e-06)$	$\log(1e-3, 1e-06)$
Warmup Epochs	3	3
Future Observation Offset	10	10
Latent Action Dimension	8192	512
<b>BC</b>		
Dropout	0	0
Use Augmentation	False	False
Evaluation Seed	0	0
Batch Size	512	64
Number of Epochs	10	10
Frame Stack	3	3
Encoder Deep	False	True
Weight Decay	0	0
Encoder Scale	32	8
Evaluation Episodes	5	5
Learning Rate	0.0001	0.0001
Warmup Epochs	0	0
Encoder Number of Residual Blocks	2	2
<b>BC finetuning</b>		
Use Augmentation	False	False
Batch Size	512	64
Hidden Dimension	256	[64, 512]
Weight Decay	0	0
Evaluation Episodes	25	25
Learning Rate	0.0003	0.0001
Total Updates	2500	15000
Warmup Epochs	0	5

Table 7: Hyperparameter optimization setup for latent action learning from images (used for **lapo**, **lapo-masks**).

Hyperparameter	DCS	DMW
<b>Latent Action Learning</b>		
Batch Size	512	64
Number of Epochs	10	10
Frame Stack	3	3
Encoder Deep	False	True
Weight Decay	0	0
Encoder Scale	6	4
Learning Rate	$\log(1e-3, 1e-06)$	$\log(1e-3, 1e-06)$
Warmup Epochs	3	3
Future Observation Offset	10	10
Latent Action Dimension	1024	1024
Encoder Number of Residual Blocks	2	[1, 2]
<b>BC</b>		
Dropout	0	0
Use Augmentation	False	False
Evaluation Seed	0	0
Batch Size	512	64
Number of Epochs	10	10
Frame Stack	3	3
Encoder Deep	False	False
Weight Decay	0	0
Encoder Scale	32	8
Evaluation Episodes	5	5
Learning Rate	0.0001	0.0001
Warmup Epochs	0	0
Encoder Number of Residual Blocks	2	[1,2]
<b>BC finetuning</b>		
Use Augmentation	False	False
Evaluation Seed	0	0
Batch Size	512	64
Hidden Dimension	256	[64, 512]
Weight Decay	0	0
Evaluation Episodes	25	25
Learning Rate	0.0003	0.0001
Total Updates	2500	15000
Warmup Epochs	0	0